Applications

The specific equipment now being fabricated (Fig. 3) is tailored to rendezvous and docking applications. With the optional target vehicle angle tracker and acquisition beacon, it will suffice for nearly all conceivable cooperative rendezvous and docking situations. It will operate automatically or will provide display information. Range rate may be easily measured to the accuracies necessary to provide automatic docking of large vehicles, a function that apparently cannot be satisfied easily by other techniques.

For certain limited applications, rendezvous may be accomplished without the optional equipment. However, for docking, the relative angular position of the target vehicle must still be known. An astronaut on board the chaser vehicle can supply this information visually, and docking can be accomplished, provided that the chaser vehicle can move laterally to obtain angular alignment. This information could also be obtained from the target vehicle via a communications link. The instrument for measuring angular position in this case would be a very small telescope focusing onto a solid-state quadrant detector.

Figure 5 shows a system that has a complete transceiver at either terminal. Two transmitters operate at slightly different wavelengths to separate radar and communication functions. The two wavelengths are separated by dichroic beamsplitters in each transceiver as indicated and directed to radar and communications detectors. The communications capability could also be provided by a physically separate receiver. Since the telescopes are so small, no great penalty would be involved.

Such a system may be applied to a variety of situations. For instance, some astronomical payloads are required to be unmanned for stability and contamination considerations. At the same time the vehicle must be controlled and monitored during acquisition and observation of astronomical objects, and also administered occasionally for maintenance or for removal and replacement of photographic supplies. Such a payload requires station-keeping by a remote satellite, with a command communication link to it and a monitoring link from the payload. With the system shown in Fig. 5, the radar can be programmed to maintain a certain range between the spacecraft, while for maintenance the payload can be commanded back to the manned satellite. In a similar manner this system can provide a station-keeping and two-way communications capability for an orbital assembly, fueling, and launch facility. Other configurations could provide a) rendezvous and docking automatically for supply shuttles to space stations or for space rescue missions, or b) station-keeping and communications link between stationary atellites and terminals on the moon or earth.

Conclusions

The addition of the wide-angle, gimballess capability of the advanced tracking technique greatly enhances the over-all versatility and performance capacity of laser radars for rendezvous and docking. Even if a particular vehicle or payload requires hemispherical coverage, it can be done with an indexed and mechanically latched gimbal system far simpler and more reliable than with precision gimbals. The wide-angle capability allows wide-angle limit-cycling in rendezvous and station-keeping applications, with a resultant large savings in fuel, and the capability for tracking high angular rates allows vehicle maneuvers to take place simultaneous to tracking.

The versatility of providing radar and communication functions on the same sensor system is a tremendous aid in station-keeping applications. Presently, bandwidths of several tens of kilobits per second can be provided. One megabit with room temperature GaAs lasers is expected within the year, and eventually these devices may be used to transmit real-time television.

Other techniques would require two or even three complete systems to provide rendezvous radar, docking radar, station-keeping, and communications systems capacity. This system is smaller, weighs less, and uses less power than any one of the other systems but can simultaneously provide all of these capabilities to most of these missions.

References

[1] Dixon, T. P., Wyman, C. L., and Coombes, H. D., "A Laser Guidance System for Rendezvous and Docking," *Navigation—The Journal of the Institute of Navigation*, Vol. 13, No. 3, Autumn 1966.

[2] Wyman, C. L., "Test Performance of an Experimental Laser Radar for Rendezvous and Docking," *The Journal of Spacecraft and Rockets*, Vol. 5, No. 4, April 1968, pp. 430–433.

[3] Fowler, V. J. et al., "Investigation of Electro-Optical Techniques for Controlling the Direction of a Laser Beam," Interim Report TR 65-722.8, General Telephone and Electronics Labs., Bayside, N. Y.

[4] Eberhardt, E. H., "Tracking Properties of ITTIL Deflectable Multiplier Phototubes," Applications Note E-3, Dec. 6, 1963, ITT.

[5] Rutz, E. M., and Edmonds, H. D., "Diffraction Limited Gallium Arsenide Laser," Final Report, FSC 68 0718/4596, Oct. 15, 1968, IBM, Gaithersburg, Md.

[6] Fowler, V. J. et al., "Investigation of Electro-Optical Techniques for Controlling the Direction of a Laser Beam," Interim Report TR 66-722.17, General Telephone and Electronics Labs., Bayside, N. Y.

Effects of Simulated Mars Dust Erosion Environment on Thermal Control Coatings

G. L. Adlon* and E. L. Rusert†
McDonnell Douglas Corporation, St. Louis, Mo.
and
W. S. Slemp‡
NASA Langley Research Center, Hampton, Va.

Nomenclature

T_e	= exposure time, min or hr
α_s	= solar absorptance
$\Delta W, \Delta t$	= weight and thickness losses, 10^{-2} g and 10^{-4} in.
ϵ_{tn}	= total normal infrared emittance
$\rho_d^* \equiv \rho_d/\rho_{do}$	= normalized dust density; $\rho_o \equiv 1.0 \times 10^{-4}$ oz/ft^3
θ	= angle between specimen surface and wind vector, deg

Introduction

THE Viking project is expected to land a vehicle on Mars in 1973 to conduct scientific experiments for 90 days. The postulated Martian environment has a solar constant of

Presented as Paper 69-1023 at the AIAA Fourth Space Simulation Conference, Los Angeles, Calif., September 8–10, 1969; submitted September 11, 1969; revision received January 26, 1970. This work was sponsored under a NASA Langley Funded Contract: NAS-1-8708, "Planetary Environment Simulation Experimental Study," Task 3-Erosion and Dust Coating Effects. The authors wish to acknowledge the assistance of T. H. Allen, J. J. Henderson, and C. R. Johnson.

* Senior Engineer, Space Simulation and Systems Laboratories, McDonnell Aircraft Company.

† Senior Engineer, Material and Processes, McDonnell Douglas Astronautics Company—Eastern Division.

‡ Aerospace Technologist, Coating and Surface Section, Chemistry and Physics Branch of the Applied Materials and Physics Division. Member AIAA.

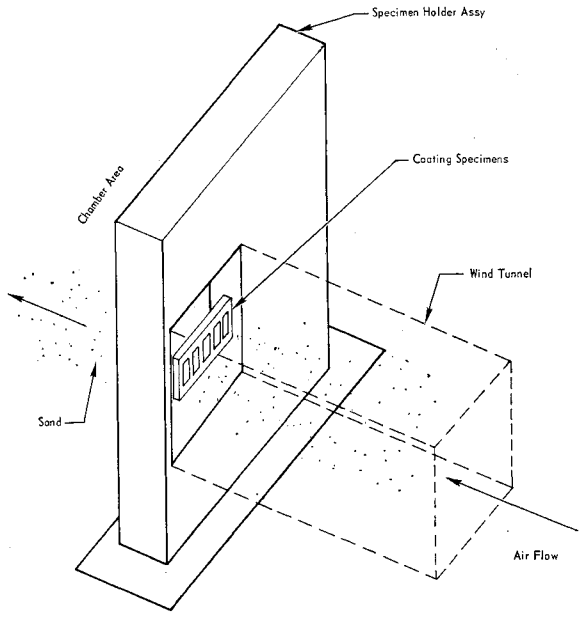

Fig. 1 Specimen holder assembly.

190 Btu/hr-ft², a surface pressure between 3 and 15 torr, and a surface temperature range of $\sim -150°$ to $+125°$F. Combinations of the low pressure and variations in temperature could theoretically generate surface wind speeds as high as 200 fps.[1,2] This Note presents the results of tests performed under simulated surface dust storm conditions on the radiative or optical properties of twelve thermal control coatings, two mirrors, and two window materials.

The tests were conducted at McDonnell in a wind tunnel, which was equipped with a sand injection system and was located in a 9 × 11 × 20-ft space chamber that was pumped by a six-stage steam ejector. The total system, including steam ejector, chamber, and tunnel, can simulate the Mars engineering model parameters.[3–5] Although wind velocity and chamber pressure can be varied, values of 220 fps and 7 torr were used for all of the present tests. Air drawn from storage tanks was filtered, dried to a dew point of $-20°$ to $-40°$F, and passed through a metering orifice, a 2-in. pipe, a diffuser, stilling screens (within the tunnel plenum), a 9.5- × 14.5-in. nozzle, and the test section. Silica sand was metered into the 2-in. pipe line between the flowmeter and diffuser. Reference dust particle density ρ_{d_0} at the tunnel outlet was 1.0×10^{-4} oz/ft³. The sand metering system consisted of a hopper with a variable orifice through which sand was gravity-fed to an endless belt (driven by a variable-speed motor), thence into a funnel and into the 2-in. air line (which is at a lower pressure). The sand particle size range (44–105μ used for all tests is within the range postulated to occur at Mars near-surface conditions.[5] Particle sizing was performed according to MIL-STD-810A requirements. The particle blowing densities used were based upon results of studies of particle saltation phenomena in simulated Martian sand storms.[3,4]

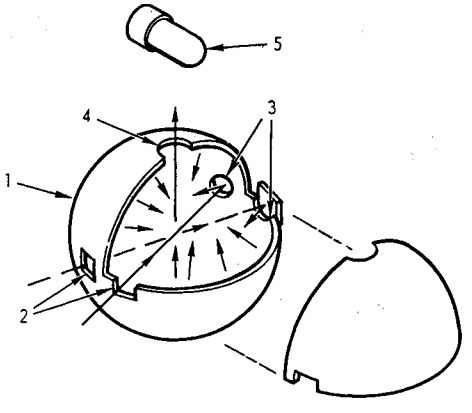

Fig. 2 Integrating sphere-optical arrangement. 1-integrating sphere, 2-entrance ports (cells are placed here for absorptance and transmittance measurements), 3-exit ports (sample and reference materials are placed here for reflectance measurements; otherwise, ports are normally covered with magnesium oxide plates), 4-integrating sphere opening, and 5-detector.

Table 1 Materials evaluated

Material	t,[a] mils	Comments
Thermal control materials		
1 Aluminized Teflon (fep type C)	5	Coated by G. T. Schjeldahl Co.
2 Gold-coated Teflon (fep type A)	2	Supplied by JPL
3 Gold-coated Kapton	5	Supplied by JPL
4 Grit-blasted 6061T6 aluminum	64	
5 Glass resin (Owens-Illinois 650) unpigmented	1	Applied to polished 2024T3 Alclad Al
6 White polyurethane	2	Desoto Inc. No. 821-010
7 Aluminum pigmented silicone	7	G. E. No. RTV 602 silicone
8 Aluminum pigmented epoxy	5	Desoto Inc. 529-004
9 Alumino-silicate pigmented glass resin	13	H-10, applied by Hughes Aircraft
10 Flame-sprayed Nickel aluminide (NiAl)	7	Metco 404[b]
11 Flame-sprayed NiAl (40%) + ZrO_2 (Zirconia, 60%)	7	Metco 413[b]
12 Plasma-sprayed Al_2O_3	16	Metco 101[b]
Reference materials		
13 Glass slides	60	
Windows		
14 Fused silica (Corning 7940)	250	Polished[c]
15 Alumino-silicate (Corning 1723)	250	Polished[c]
Mirrors		
16 Fused silica, aluminized and quartz-overcoated	125	Second-surface mirror (General Electric 151 silica)
17 Soda lime, aluminized and quartz-overcoated	250	First-surface mirror (Liberty Mirror)

[a] For specimens 1–3 and 5–12 this is coating thickness; substrate for all coatings is 6061T6 aluminum.
[b] Applied by NASA Langley.
[c] To $\frac{1}{4}$ wavelength, wedge angle <30 sec.

The specimen holder assembly (Fig. 1), located at the tunnel exit, consisted of six individual specimen holders mounted on a remotely controlled motor-driven, rotatable shaft. Each holder held five 2 × 2-in. coating specimens. The six holders were contained within a housing that allowed only one holder to be exposed to the environment at a time. Thus, as many as 30 specimens could be tested without shutting down the wind simulator system.

Material Selection and Test Procedure

At the time of material selection, the Mars lander design requirements for thermal control coatings and optical materials had not been determined; therefore, the coatings (Table 1) were selected on the basis of predicted wear resistance and known radiative properties. Earlier studies[6] had shown that the wear resistance of pigmented thermal control coatings is a function of the binder system used in the coating formulation. In view of this, a group of coatings was chosen for use in these tests on the basis of their binders (materials 5–9 in Table 1). The results of these tests could allow selection of other pigments to optimize radiative properties.

The coatings were tested in groups of four with a glass slide as a reference specimen evaluated with each group. After a timed exposure another group was moved into the test zone by remote control, thereby maintaining constant test parameters in the chamber for each set of specimens. The coatings

Table 2 Changes in coating weight (ΔW, 10^{-2} g) and thickness (Δt, 10^{-4} in.) from test at 7 torr in 220 fps wind[a]

Material (Table 1)	θ = 45°, T_e = 2 hr, ρ_d* = 1.0		90°, 2 hr, 1.0		90°, 2 hr, 1.45		90°, 4 hr, 1.5	
	ΔW	Δt	ΔW	Δt	ΔW	Δt	ΔW	Δt
1–5	0	0	0	0	0	0	0	0
4	0	0	0	2	0	2	0	3
6	0	3	0	10	0	12	0	2
7	0	2	0	0	0	1	0	0
8	1	1	1	2	1	3	1	7
10	7	10	7	9	7	11	12	15
12	8	11	15	14	19	6	47	36
11	11	12	14	2	16	5	17	8
9	17	35	19	34	21	38	31	46
13	1	0	4	2	4.7	3	10	7

[a] Test specimens were cleaned with compressed nitrogen and a soft nylon brush prior to measurements.
[b] Average of three tests.

were subjected to four combinations of orientation angle θ (45° or 90°), exposure time T_e (2 or 4 hr) normalized and dust densities, $\rho_d^* = \rho_d/\rho_{d_o}$, of 1.0 and 1.5, as shown in Table 2. The α_s and ϵ_{t_n} were measured after exposure in both the dusty condition (as removed from the test chamber) and the clean condition (dust removed with compressed nitrogen and soft nylon brush) (Table 3). The (Table 2) weight and thickness changes were measured in the clean condition.

The optical materials were exposed at $\theta = 90°$, $\rho_d^* = 1.5$, for T_e = 5–20 min. Both the diffuse transmittance (DT) and the diffuse plus specular transmittance (DST) over a wavelength range of 650–2750 were measured. These measurements were made with a Beckman DK-2A Spectrometer equipped with an integrating sphere reflectometer. The DST was measured by placing the sample in front of the sample beam entrance port on the integrating sphere (Fig. 2) with M_gO-coated plates in both the exit reference and sample positions. This arrangement utilizes the light transmitted by the sample over a complete hemisphere. The DT was measured by removing the opposite M_gO-coated plate, which permitted the specular component to leave the integrating sphere exit port. In this case only the scattered light incident on the wall of the integrating sphere is utilized for the measurement. Lines for 0 and 100% were established on the spectrometer chart by comparing two identical smoked M_gO plates. Reflectance measurements on the mirrors were made with the sample replacing the M_gO plate in the sample beam.

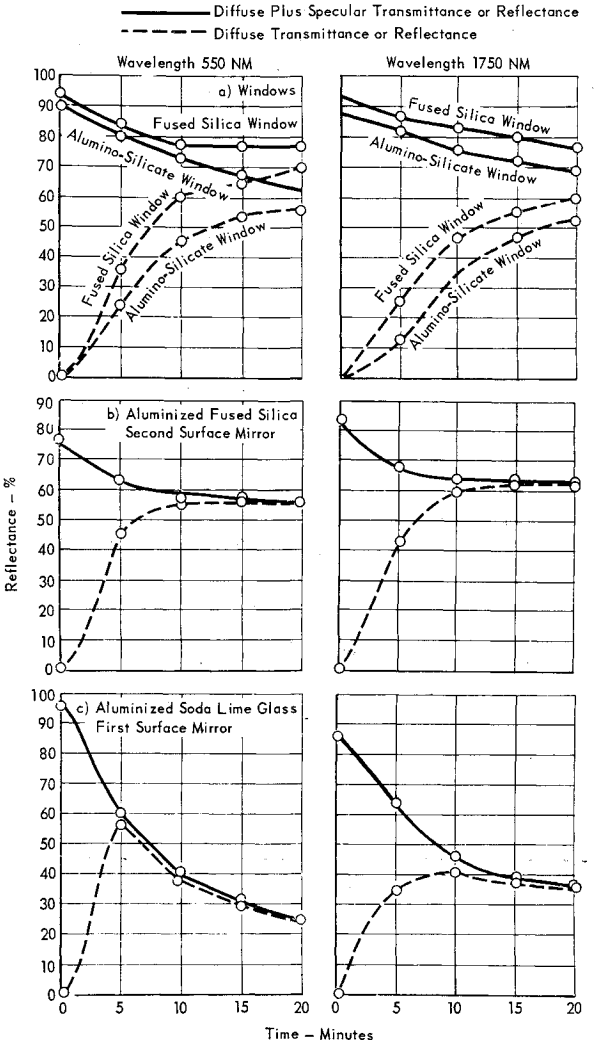

Fig. 3 Transmittance (for windows) and reflectance (for mirrors) vs exposure time.

Scattering of light by a mirror was measured by positioning the mirror in the sample exit port so that the beam was reflected back on itself and out the port. Only the light scattered out of the reflected beam and incident on the wall of the integrating sphere was detected with this technique.

Table 3 Solar absorptance α_s, emittance, ϵ_{t_n}, and α_s/ϵ_{t_n} for 7-torr, 220 fps, tests at $\theta = 90°$

Test	Parameter[a]	Material number 9	1	12	5	6	2	3	7	8	4	11	10
Initial data	α_s	0.16	0.24	0.27	0.33	0.33	0.41	0.51	0.51	0.52	0.68	0.84	0.86
	ϵ_{t_n}	0.93	0.77	0.93	0.75	0.89	0.65	0.82	0.44	0.47	0.25	0.62	0.58
	α_s/ϵ_{t_n}	0.17	0.31	0.32	0.42	0.38	0.62	0.63	1.15	1.10	2.76	1.36	1.48
T_e = 2 hr	α_s, u	0.27	0.45	0.34	0.44	0.55	0.57	0.73	0.78	0.76	0.65	0.78	0.78
ρ_d* = 1.0	α_s, c	0.24	0.46	0.33	0.43	0.55	0.55	0.72	0.76	0.76	0.66	0.78	0.78
	ϵ_{t_n}, c	0.93	0.76	0.83	0.66	0.85	0.66	0.83	0.71	0.67	0.36	0.46	0.45
	α_s/ϵ_{t_n}, c	0.26	0.60	0.49	0.65	0.66	0.86	0.84	1.08	1.14	1.81	1.70	1.74
T_e = 2 hr	α_s, u	0.41	0.53	0.41	0.49	0.69	0.62	0.80	0.80	0.81	0.69	0.80	0.79
ρ_d* = 1.45	ϵ_{t_n}, u	0.93	0.77	0.83	0.76	0.90	0.65	0.84	0.72	0.71	0.40	0.50	0.49
	α_s/ϵ_{t_n}, u	0.44	0.69	0.47	0.65	0.77	0.95	0.96	1.12	1.15	1.73	1.59	1.61
	α_s, c	0.30	0.51	0.39	0.46	0.63	0.60	0.79	0.79	0.81	0.70	0.80	0.79
	ϵ_{t_n}, c	0.91	0.76	0.83	0.75	0.89	0.67	0.83	0.71	0.68	0.41	0.48	0.47
	α_s/ϵ_{t_n}, c	0.33	0.67	0.54	0.62	0.71	0.95	0.90	1.12	1.20	1.72	1.69	1.69
T_e = 4 hr	α_s, u	0.39	0.67	0.46	0.50	0.72	0.71	0.86	0.85	0.84	0.72	0.79	0.78
	ϵ_{t_n}, u	0.90	0.79	0.86	0.79	0.91	0.70	0.83	0.72	0.79	0.43	0.51	0.51
ρ_d* = 1.5	α_s/ϵ_{t_n}, u	0.43	0.85	0.54	0.64	0.79	1.04	1.01	1.18	1.08	1.69	1.55	1.69
	α_s, c	0.32	0.65	0.41	0.49	0.68	0.67	0.82	0.84	0.84	0.72	0.79	0.77
	ϵ_{t_n}, c	0.93	0.75	0.86	0.77	0.92	0.69	0.85	0.72	0.74	0.43	0.47	0.47
	α_s/ϵ_{t_n}, c	0.34	0.86	0.47	0.65	0.73	0.97	0.98	1.17	1.13	1.68	1.67	1.68

[a] u = measurements of dusty, uncleaned specimens; c = measurement of specimen after cleaning with compressed nitrogen and soft nylon brush.

Results and Discussion

Neither a weight loss ΔW nor a thickness loss Δt was detected for coatings Teflon, Kapton, or glass resin coatings, and no weight loss was detected for silicone, polyurethane, or the substrate aluminum (specimen 4, Table 2). The very hard coatings (flame-sprayed NiAl, plasma-sprayed Al_2O_3, and glass reference slides) and the soft H-10 coating (highly pigmented) did experience significant ΔW's and Δt's. At a given ρ_d*, the change in θ from 45° to 90° had no effect on ΔW except for the Al_2O_3 and the glass reference slide, both of which had greater weight losses at 90°. Increasing ρ_d* from 1.0 to 1.45 with $\theta = 90°$ did not cause any appreciable increase in ΔW of any materials tested, including the glass reference materials. Increasing T_e from 2 to 4 hr, with about the same ρ_d* (1.5) and a 90° orientation, did increase ΔW for the flame and plasma-sprayed coatings and the H-10 coating. Except for the glass reference materials, increasing T_e from 2 hr to 4 hr did not produce a 100% increase in ΔW for the hard materials.

The α_s and ϵ_{t_n} changes are given in Table 3. With the exception of the flame-sprayed NiAl and NiAl + ZrO_2, and the grit-blasted aluminum, a large increase in α_s occurred when ρ_d* was increased from 1.0 to 1.5 or T_e was increased from 2 hr to 4 hr. The flame-sprayed coatings, originally porous and rough, were smoother after testing. Their increased α_s may be explained by the possibility of silica dust pickup that did not get removed by the cleaning procedure. The metallized films (aluminum-Teflon, gold-Teflon and gold-Kapton) increased in α_s as the exterior surface was etched or contaminated (silica dust pickup); this produced a diffuse surface coating over the metallized film. The unpigmented glass resin was etched by the dust, thereby producing a diffuse surface. The grit-blasted aluminum (6061-T6 alloy) surface became smooth. These results for the selected window materials and mirrors are plotted as reflectance or transmittance vs T_e in Fig. 3 for two wavelengths. In Fig. 3a, the difference between the upper (DST) curve and the lower (DT) curve in Fig. 3 is the amount of incident light usable to form an image. For $T_e \geq 15$ min, less than 15% of the incident light reaches the image. The initial test data (Fig. 3) indicate that the harder alumino-silicate is a better window material than the fused silica for the sand/dust erosion environment. The alumino-silicate has a Knoop hardness (100-g load) of 595 kg/mm² as compared to 560 kg/mm² for fused silica. For $T_e = 5$ min, the difference between the DST and DT values for the alumino-silicate is 56%, as compared to 46% for the fused silica material.

No resolution measurements were made on the mirrors. If the mirror reflectance and scattering for Figs. 3b and 3c are interpreted in the same manner as for window transmittance, it is evident that little light is available for formation of an image. The mirrors were slightly less degraded in the infrared (1750) than in the visible region (550). The second-surface mirrors (Fig. 3b) were physically more durable than the first-surface mirrors (Fig. 3a), but it should be noted that incident light passes through the damaged front surface of a second-surface mirror twice.

Conclusions

The erosion of the hard materials (flame-sprayed coatings and the glass references) increased as exposure time and dust density increased. The more resilient coatings (Teflon, Kapton, polyurethane, elastomeric silicone, etc.) did not exhibit any weight loss under any test conditions. Large increases in α_s, due to dust pickup and/or changes in surface roughness, were experienced by all coatings except the flame-sprayed nickel aluminide-type coatings. The NiAl-type coatings were the only ones to exhibit a decrease in ϵ_{t_n}; all other coatings exhibited either increased ϵ_{t_n} or no change in ϵ_{t_n}. Consequently, even though most of the coatings suffered an increase in α_s, the α_s/ϵ_{t_n} ratio for a number of them remained in the useful 0.40–0.70 range.

The specimens with initially lower α_s/ϵ_{t_n} (H-10 and plasma-sprayed Al_2O_3) had the smallest change in α_s/ϵ_{t_n}, possibly because the more resilient surfaces retain impacted silica instead of eroding away. The H-10 and plasma-sprayed Al_2O_3 erode and thus always present a clean surface. Since the solar constant for Mars is 190/Btu/hr-ft² (less than one-half that of Earth), a coating with $\alpha_s/\epsilon_{t_n} \simeq 0.70$ (with $\epsilon_{t_n} = 0.80$) could possibly be utilized on a vehicle without having it overheat when on the Martian surface; thus, it appears probable that further work will produce a suitable thermal control coating for a vehicle operating on the surface of Mars.

For window materials exposed more than 10 min and mirrors exposed more than 5 min, the amount of radiation available for image formation is significantly decreased. This results in a serious loss in resolution, especially at low contrast levels. The brightness of an image, as observed with a first surface mirror, was less than 10% of the true brightness. For windows exposed more than 10 min, the brightness was less than 15% in the visible (550) and less than 25% in the infrared (1750) regions.

References

[1] Stone, I., "Atmospheric Data to Alter Voyager Design," *Aviation Week and Space Technology*, Vol. 83, No. 21, Nov. 22, 1965.

[2] Christian de Wys, E., "The Surface of Mars," 1968, Jet Propulsion Lab., Pasadena, Calif.

[3] Hertzler, R. G., "Behavior Characteristics of Simulated Martian Sand and Dust Storms," Rept. E720, Aug. 1966, McDonnell Aircraft Co., St. Louis, Mo.

[4] Hertzler, R. G., Wang, E. S. J., and Wilbers, O. J., "Martian Sand and Dust Storm Experimentation," *Journal of Spacecraft and Rockets*, Vol. 4, No. 2, Feb. 1967, pp. 284–286.

[5] "Mars Engineering Model Parameters for Mission and Design Studies," May 1968, NASA.

[6] Rusert, E. L. and Wilbers, O. J., "Effects of Spacecraft Sterilization Procedures and Mars Environment on Thermal Control Coatings," *The Effects of Space Environment on Materials*, Vol. 11, Western Periodicals, North Hollywood, Calif., April 1967, pp. 63–73.

A Study of the Nonlinear Rolling Motion of a Four-Finned Missile

PETER DANIELS*
Naval Weapons Laboratory, Dahlgren, Va.

Nomenclature

C_l = aerodynamic rolling moment coefficient
C_{l_p} = aerodynamic roll damping coefficient
$C_{l\delta}$ = C_l derivative due to fin cant
$C_{l_{4\gamma}}$ = induced rolling moment coefficient for a four-finned missile
d = missile reference diameter
I_x = axial moment of inertia
N = number of fins
p = spin rate
Q = dynamic pressure
S = reference area
V = missile velocity
α = angle of attack
γ = angle between reference fin and normal component of missile velocity
δ = fin cant angle

Received October 22, 1969; revision received January 12, 1970. Acknowledgement is due C. J. Cohen, Research Associate for the Warfare Analysis Department, who first suggested that the roll damping at high angles of attack could be expressed as a cubic. Equation (5) is also due to him.

* Research Scientist, Warfare Analysis Department.